MINERALOGY, CHEMISTRY, AND DISTRIBUTION OF SELECTED TRACE ELEMENTS IN COAL AND SHALE FROM THE IBAR BASIN (SOUTH SERBIA)

by

Željana N. NOVKOVIĆ[a], Nenad T. NIKOLIĆ[b], Nevena A. ANDRIĆ-TOMAŠEVIĆ[c], Violeta M. GAJIĆ[d], Mercedes SUAREZ[e], Emilia GARCIA-ROMERO[f], Vladimir M. SIMIĆ[d], and Dragana R. ŽIVOTIĆ[d]*

[a]MMI Bor Mining and Metallurgy, Bor, Serbia
[b]Institute for Multidisciplinary Research, University of Belgrade, Belgrade, Serbia
[c]Institute of Applied Geosciences, Karlsruhe Institute of Technology, Karlsruhe, Germany
[d]Faculty of Mining and Geology, University of Belgrade, Belgrade, Serbia
[e]Department of Geology, University of Salamanca, Salamanca, Spain
[f]Department of Mineralogy and Petrology,
Complutense University of Madrid and Geosciences Institute (IGEO), Madrid, Spain

Original scientific paper
https://doi.org/10.2298/TSCI240405143N

Coal samples from the Jarando, Tadenje, and Progorelica mines and organic-rich shale samples from the Piskanja boron deposit, all located in the Tertiary Ibar Basin, were studied using several methods such as transmitted light microscopy, X-ray powder diffraction (XRD), scanning electron microscopy with energy dispersive X-ray spectroscopy (SEM-EDS), Fourier-transform infrared spectroscopy (FTIR), as well as inductively coupled plasma-mass spectrometry (ICP-MS) and X-ray fluorescence (XRF) spectrometry for evaluating their mineralogical and geochemical compositions. The Ibar Basin hosts high-volatile bituminous coal deposits and boron mineralisations. The mineralogical and geochemical data indicated that the main minerals in coals are quartz, pyrite, with a variable amount of clay (kaolinite, montmorillonite, illite), calcite and sulphates, while borates occur in low amounts. Framboidal pyrite is the main form of sulphur in coals. Clay and carbonate are often associated with macerals in mineral-bituminous groundmass, implying high ash yield and limited possibilities of coal cleaning treatment. Very high content of As, Co, Cu, Cr, and Ni was detected in high temperature coal ash (HTCA), especially in the Tadenje deposit. Contents of Mo, Sb, Pb, V, and Zn are slightly higher than the relevant Clarke values for bituminous coal ash. The shale samples from the Piskanja deposit mostly consist of a mixture of quartz, dolomite, and clay minerals (illite and chlorite) with variable amount of plagioclase, K-feldspar, and mica. Lead, Zn, and Cu sulphides, gypsum, celestine, barite, rutile, and apatite were detected in low amounts.

Key words: *Ibar Basin, bituminous coal, shale, mineralogy, trace elements*

Introduction

Coal is a very complex natural material consisting of a mixture of organic (macerals) and inorganic (minerals) components, gases and liquids at variable contents. The origin and the

* Corresponding author, e-mail: dragana.zivotic@rgf.bg.ac.rs

chemical properties of all components depend on the depositional environment, namely the conditions dominated in the paleomire, and the degree of chemical transformation the original sediment (peat) underwent, called coalification. The amount and the mode of occurrence of the inorganic components (minerals and elements) contained in coal [1], affect its quality and provide valuable information on its behaviour during both mining and utilisation [2]. The determination of mineral and chemical composition of coal is very important for an effective coal utilisation [3].

The Serbian bituminous coals are of minor economic importance due to their low quality and complex geological setting, the latter causing hard exploitation conditions. Today bituminous coal is mined only in the Ibar Basin (low-rank bituminous) and at Vrška Čuka (high-rank bituminous). The Ibar Basin is situated about 200 km south of Belgrade, in southern Serbia (fig. S1 in the *Supplementary material*). The basin is distinguished into several subbasins (Ušće, Tadenje, Jarando, Gradac) filled with Lower Miocene coal-bearing terrestrial sedimentary rocks [4, 5]. Bituminous coal is exploited in the Jarando and Tadenje underground mines and in the Progorelica open pit. Recent research confirmed the rank of the coal and shale of the Ibar Basin [6]. Previous exploration of the Ibar Basin focused on geology, stratigraphy, sedimentology, and coal properties, necessary for exploitation [7-11]. Mineralogical studies of coal and related sedimentary rocks, *e.g.* shales, were rarely conducted. The aim of this paper is to provide information on the mineralogical composition of Ibar coal and shale samples, as well as on the content of major and selected trace elements in high temperature coal ash.

Geological setting

The Ibar Basin is part of the Neogene Lake system placed in the internal part of the Dinarides [12, 13] which are formed during the collision of the European and Adriatic plates [14]. The Dinarides were affected by large-scale extension during Miocene [15, 16]. The Miocene extension led to exhumation of deep-seated core-complexes (*e.g.* Studenica and Kopaonik core-complex [15, 17]), as well as to the formation of extensional basins in the hanging wall, like Ibar Basin, [6].

The basement of the Ibar Basin consists of Palaeozoic chlorite schist; Triassic limestone, dolomite, marble, sandy marlstone, and marlstone; Jurassic harzburgite, serpentinite, gabbro, rodingite, and other rocks of the ophiolite melange; Oligocene/Miocene dacite-andesite lava flows; and Neogene quartzlatite/rhyodacite extrusions and pyroclastic rocks. Sedimentary rocks mainly of Neogene age consist of conglomerate, sandstone, marlstone, coal, carbonaceous shale, shale, and claystone.

The Lower Miocene Ibar Basin hosts mainly clastic to carbonate rocks including three to nine high-volatile bituminous coal seams. The deposition started in shallow lakes and mires at the earliest stage, later in alluvial and at the latest phase in the lacustrine environment [5]. Basin subsidence resulted in the formation of a 1500 m thick sedimentary sequence (based on geophysical exploration) [5].

The basin hosts bituminous coals, boron mineralization (borates and howlite), magnesite deposits and travertine, the latter is noticed during previous investigation [6]. The relatively high rank of Tertiary coals from the Ibar Basin is due to thermometamorphism, while the differences in maceral and geochemical composition of Tadenje coal were explained by relatively more oxic depositional environment [4]. The age of sediments is not well constrained. Based on sedimentary layer correlation from other intermontane basins in the Dinaridic Lake System, it could be inferred that the alluvial deposition started around 19-17 Ma (Megaannum)

and lasted until 16-15 Ma when a typical lacustrine environment established. Combining geodynamical [17] and paleontological lines of evidence in the following discussion [6], 19 Ma was adopted as the age of the onset of sedimentation in the Ibar Basin.

Vitrinite reflectance and apatite fission track data of the studied sedimentary rocks from the Piskanja (IBM-1) and Tadenje deposits imply post-depositional thermal overprint in the Ibar Basin. Thermal history models of the detrital apatite [6] revealed a heating episode prior to cooling that began at around 10 Ma. The heating episode started around 17 Ma and lasted until 10-8 Ma reaching maximum temperatures between 100-130 °C. Authors correlate this event with the domal uplift of the Studenica and Kopaonik core complex. The cooling episode is related to basin inversion and erosion. The apatite fission track data indicates local thermal perturbations, detected in the SE part of the Ibar Basin (Piskanja deposit) at around ~7.1 May, which may correspond to the youngest hydrothermal phase in the region.

Samples and analytical methods

Thirteen coal samples were collected through channel sampling from the Jarando, Tadenje, and Progorelica mines. Moreover, nine shale samples were picked up from the IBM-1 core drilled in the Piskanja deposit (tab. S1 and fig. S1 in the *Supplementary material*). The samples represent different lithotypes and parts of the coal seams.

The sedimentological examinations included several analytical procedures required for the optical determination of mineralogical-petrographical composition. About 30 g of each sample were poured into distilled water, slowly heated up to 40 °C for 30 minutes, and treated in an ultraviolet bath for 30 minutes. After cooling at room temperature, the sample was wet sieved using mesh with 0.063 mm openings. The fraction above 0.063 mm has been dried at room temperature and treated further. The next step is the split into two fractions using mesh with 0.6 mm openings, getting two fractions, one > 0.6 mm and the other < 0.6 mm. The > 0.6 mm fraction was used for thin section preparation. The < 0.6 mm fraction was subjected to heavy liquid separation using bromoform of specific mass 2.87 g/cm^3. From the heavy fraction the magnetic minerals (magnetite, pyrrhotine) were removed by hand magnet. Optical tests were performed using binocular lens with integrated led light and digital camera Leica E34D and on thin sections prepared in xylol [18] using the polarized microscope DMLSP connected to digital camera Leica DC 300. The sedimentological examinations were performed on samples Jarando 1, Jarando 3, Tadenje 11, Tadenje 1, Tadenje 10B, Progorelica 3, Progorelica 1, Progorelica 10, and Progorelica 16.

The XRD analysis was performed on coal samples (tab. S1) using a Rigaku SmartLab multipurpose X-ray diffractometer system in θ-θ geometry (the sample in horizontal position) in para-focusing Bragg-Brentano geometry using D/teX Ultra 250 strip detector in 1D XRF suppression mode with K_β-filtered $CuK_{\alpha 1,2}$ radiation source (U = 40 kV and I = 30 mA). The XRD patterns were collected in a continuous scanning mode in 2θ range 5-90°, with a step of 0.01° and data collection speed of 0.4° per minute. For shale samples from the Piskanja boron deposit, tab. S1, XRD was performed on: whole rock powdered, untreated oriented sample, and glycolated-oriented sample. The < 2 μm sample was obtained by suspension in water, decantation and studied as oriented aggregates under ambient conditions and after solvation with ethylene glycol. Treated samples were studied with a step velocity of 0.05° every 3 seconds, from 2° to 65° in the case of the powdered whole rock and from 2° to 15° in the different oriented aggregates, with a step velocity of 0.05° each second. A Siemens D-500 XRD diffractometer with a CuKα radiation and a graphite monochromator was used. The crystal phase identification

of all samples was performed in dedicated RIGAKU PDXL 2.0 software (with implemented ICCD PDF-2 2016 database).

The FTIR spectra of the thirteen powdered coal samples, tab. S1, were recorded using a Perkin Elmer Spectrum Two equipped with the Universal ATR accessory. The spectrum of each powder sample was recorded in the mid-infrared range 4000-400 cm^{-1} with 20 scans and a spectral resolution of 4 cm^{-1}. Baseline correction and band position determination were performed using the SPECTRAGRYPH software [19]. The band assignment was performed through comparison with the reported data on analogous material.

The mineral composition of selected coal and shale samples, tab. S1, was investigated using a JEOL JSM-6610LV SEM (30 kV accelerating voltage) equipped with an energy-dispersive X-ray spectrometer (SEM-EDS; X-Max Large Area Analytical Silicon Drift connected with INCAEnergy 350 Microanalysis System). Polished blocks of selected samples prepared according to standard procedure [20], were coated with a thin gold film for a higher quality of secondary electron image for SEM and EDX examination.

The contents of major elements in shale samples were determined by XRF, while these of trace elements were determined by ICP-MS. Major and trace elements of coal ash samples were analysed by inductively coupled plasma – atomic emission spectrometry (ICP-AES). The XRF analysis was performed on RIGAKU Super Mini 200 XRF analyzer. Dried samples have been heated at 1000 °C. After cooling 2.5 g of each sample and 6 g of solvent made of Li-tetraborate and Li-metaborate (3:1), were homogenised and furnaced. The contents of minor elements in the shale samples were performed by ICP-MS analysis on Agilent 7700 following the procedures outlined by ASTM D6357-21a [21] standard. Major and minor elements in coal ash samples were determined by Spectro Ciros ICM-AES following the procedures outlined by ASTM D6349-21 [22] standard. For digestion, 0.2-0.5 g of powdered ($\varnothing$ < 150 μm) ash sample was weighed into a 100 mg or 200 mg Teflon beaker. About 20 mL of aqua regia and 20 mL of concentrated HCl were added to the beaker. The beaker was heated to 130 °C to 150 °C. After the solution evaporated the beaker was removed and cooled to room temperature. Then 1 mL of concentrated HNO_3 and 20 mL of H_2O were added to the beaker and heated at 90 °C to 100 °C. The solution was cooled at room temperature and diluted with water.

Results

Mineralogy

Sedimentology

The heavy fraction of coal from the Jarando Basin consists of magnetite, sulphides, rounded aggregate grains, rock fragments, and coal fragments with sulphides, fig. 1. In the Jarando 1 sample, fragments of black coal with small radial minerals, probably borates, were separated. Pure minerals such as garnet and tourmaline, are rarely present. The light fraction dominantly consists of coal fragments. Inorganic constituents are represented by quartz or quartzite, rock fragments, borates, and rare feldspar grains.

Magnetite, rare sulphides and coal fragments with sulphides, as well as rock fragments, were determined in the heavy fraction of coal from the Tadenje deposit. In the magnetic fraction, individual grains of rock/mineral fragments being heavily impregnated with small magnetite crystals and borates with a specific density higher than 2.87 g/cm^3, were separated. Sulphide aggregates are in association with borates in radial forms, fig. 1(a). Fragments of marly rocks with borate laminae are more common here. The heavy fraction very rarely contains garnets, rutile, and dolomite. The light fraction consists mainly of coal fragments. There

are also fragments of rocks with borates in the form of thin laminae or radial minerals. Other constituents in the light fraction are calcite/dolomite aggregate grains and rarely, quartz and feldspars.

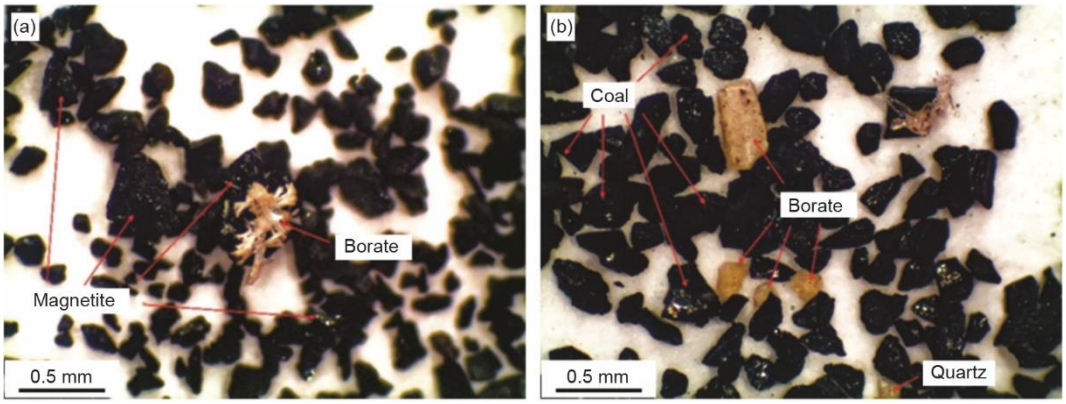

Figure 1. Photomicrographs of (a) the heavy fraction with magnetite, rock fragments and borates in Progorelica deposit and (b) the light fraction with coal fragments, borates, and quartz in Jarando deposit (the Ibar Basin). Photomicrographs were taken under reflected white light

In the Progorelica deposit magnetite, rarely sulphides and coal fragments with sulphides and borates, as well as fragments of felsic volcanic and fine grained sedimentary rock, are included in the heavy fraction. Hornblende, siderite, garnet, rock fragments, and tourmaline also occur in small amounts. The light fraction is mainly made up of coal fragments. There are also fragments of marly and dolomitic claystone with borates in the form of thin laminae or radial minerals. Other constituents in the light fraction are calcite/dolomite aggregate grains and rarely, quartz and feldspars.

The X-ray diffraction analysis

The XRD analysis proved that the mineral matter in the Jarando and Progorelica coals mainly consists of quartz, tab. 1 and fig. 2, with variable contents of kaolinite, montmorillonite, illite, and pyrite. The most abundant minerals in the Tadenje Seam-3 coal are quartz and pyrite, while kaolinite, calcite, gypsum, szomolnokite [$FeSO_4 \cdot (H_2O)$]/kieserite [$MgSO_4 \cdot (H_2O)$], montmorillonite and illite are less abundant. Calcite is the most abundant mineral in the lower part of coal Seam 6 in Tadenje deposit with variable amounts of pyrite, quartz, kaolinite, and szomolnokite/kieserite. Illite and interstratified smectite-chlorite/vermiculite are less abundant. Analcime was observed in low amount only in Tadenje 1 sample.

Quartz was identified as the most dominant phase in shales from Piskanja boron deposit, tab. 1, fig. 2. Dolomite was observed in IBM-1/2, showing very low intensity peak in IBM-1/4. Traces of ankerite were detected only in sample IMB-1/2. Illite and/or mica, and chlorite occur in all samples. The XRD patterns of several shale samples in untreated, oriented and glycolated samples indicate the presence of the interstratified swelling + non-swelling components in mixed-layered clays, either as regularly interstratified smectite-chlorite or smectite-vermiculite (samples IBM-1/3, IBM-1/7, IBM-1/8). Mixed-layered clay minerals of randomly interstratified illite+smectite or illite+vermiculite were identified in two samples (IBM-1/2 and IBM-1/4). Plagioclase occurs in all samples, generally in small amounts. The low content of

pyrite was observed in two samples (IBM-1/4 and IBM-1/27). Zeolite of clinoptilolite-heulandite group was identified only in sample IBM-1/8.

Table 1. Mineralogical composition of coal and shale samples from the Ibar Basin, based on XRD data

Sample ID	Qz	Ilt	Mnt	Kln	Chl	Ms/ Ilt	INT Sme-Ilt	INT Sme-Chl/Vrm	Cal	Dol	Ank	Py	Gp	Szo/ Kie	Pl	Cpt/ Hul	Anl
Jarando 1	M		m	m								m					
Jarando 3	M		m	m								m					
Tadenje 11	M	l	l	l								m	m				
Tadenje 14	M		l						l			m	l	m			
Tadenje 1	M		l					l	m			m		m			l
Tadenje 10A	m	l		l					M			m	l	l			
Tadenje 10B	m	l							M			m	l	m			
Progorelica 3	M			m													
Progorelica 5	M		m	m													
Progorelica 1	M																
Progorelica 10	M		m	m								m					
Progorelica 16	M		m	m								m					
Progorelica 11	M		m	m													
IBM-1/2	M				l	l	l			m	l				l		
IBM-1/3	M				l	l		l							l		
IBM-1/4	M				l	l	l					l			m		
IBM-1/7	M				l	l		l							l		
IBM-1/8	M				l	l		l							m	l	
IBM-1/27	M				l	l						l			m		

Abbreviations [23]: Qz – quartz, Ilt – illite, Mnt – montmorillonite, Kln – kaolinite, Chl – chlorite, Ms/Ilt – muscovite/illite, INT Sme-Ilt – interstratified smectite-illite, INT Sme-Chl/Vrm – interstratified smectite-chlorite/vermiculite, Pl – plagioclase, Cal – calcite, Dol – dolomite, Ank – ankerite, Py – pyrite, Gp – gypsum, Szo/Kie – szomolnokite/kieserite, Cpt/Hul – clinoptilolite/heulandite, M – most abundant, m – medium abundant, l – less abundant.

The SEM-EDS analysis

The SEM-EDS examination revealed that the most abundant minerals in coal samples from the Jarando, Progorelica and most samples from Tadenje are quartz, clay minerals (illite, kaolinite, fig. 3) and pyrite. Calcite is abundant in two coal samples from Tadenje deposit and less abundant in Jarando and Progorelica coals. Barite and gypsum were occasionally identified in all three deposits. Other minor minerals such as rutile, hematite, biotite, boehmite, and sphalerite were observed in a few coal samples. Diatoms were observed in Tadenje 11 sample, fig. 3. In the Jarando coal strontium, Sr, in barite and vanadium, V, in rutile were detected.

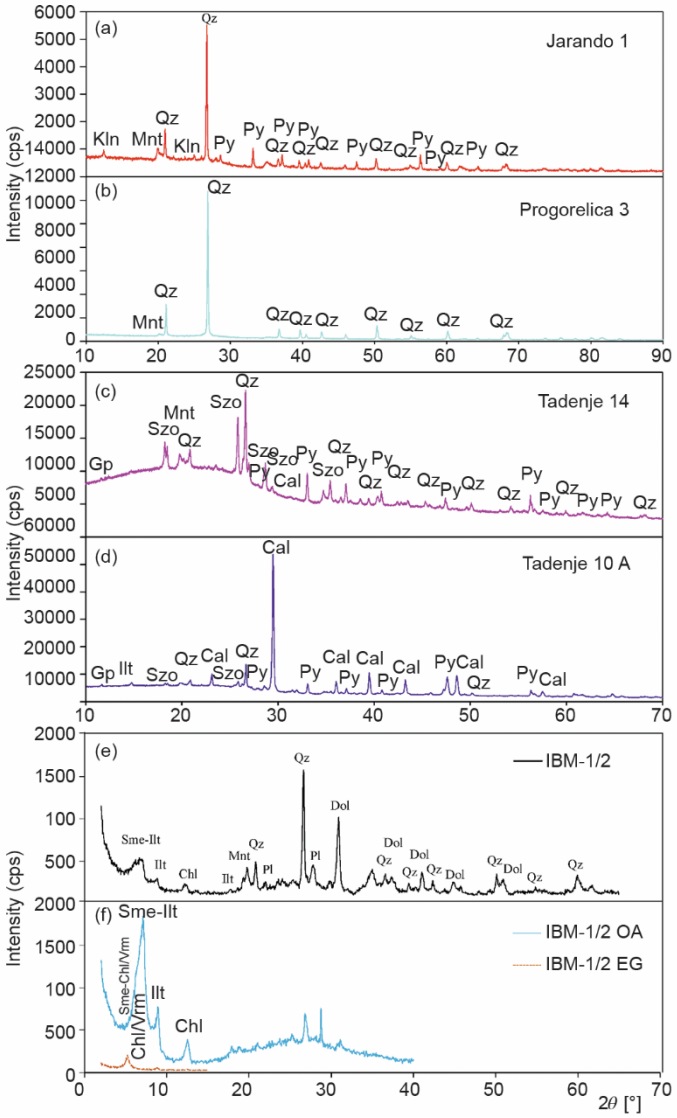

Figure 2. The XRD patterns of coal and shale samples from the Ibar Basin; (a), (b), (c), (d), (e) whole-rock samples, (f) OA – untreated oriented sample, (f) EF – glycolated-oriented sample. Abbreviations [23]: *Qz – quartz, Ilt – illite, Mnt – montmorillonite, Kln – kaolinite, Chl – chlorite, Sme-Ilt – interstratified smectite-illite, Sme-Chl/Vrm – interstratified smectite-chlorite/vermiculite, Pl – plagioclase, Cal – calcite, Dol – dolomite, Py – pyrite, Gp – gypsum, Szo – szomolnokite/kieserite*

The SEM-EDS analysis of the shale samples from borehole IBM-1 in the Piskanja deposit revealed that they mostly consist of a mixture of dolomite, fig. 3, and mica/clay minerals, as well plagioclase and K-feldspars, quartz and, rarely, minerals originating from ophiolites. Illite, and chlorite are the most abundant clay minerals. Pyrite is detected in most samples, also Pb, Zn, and Cu sulphides along with gypsum and celestine were detected in the deeper parts of the basin.

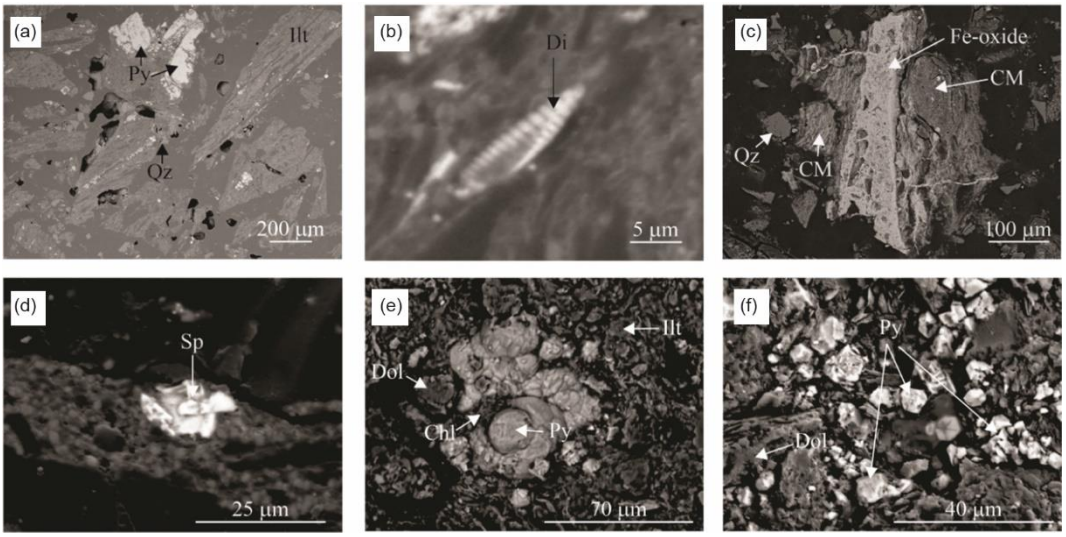

Figure 3. The SEM backscatter images of minerals in coal (a)-(d) and shale (e)-(f) from the Ibar Basin. Abbreviations [23]: *Qz – quartz, Ilt – illite, Chl – chlorite, CM – clay minerals, Dol – dolomite, Py – pyrite, Sp – sphalerite, Di – diatoms*

The Fourier-transform infrared spectroscopy analysis

The FTIR was used for profiling the coal and shale samples components. The FTIR spectra of the coal and shale samples are shown in fig. 4 and the bands position, second-derivative, assignation, and related references are given in tab. S2 and S3 (in the *Supplementary material*). The spectral data obtained show the superposition of both organic and mineral components.

Quartz is the most abundant mineral in all coal samples, fig. 4. Clay component is polymineralic, made up of kaolinite, dioctahedral smectite, and illite. In Tadenje deposit, calcite and gypsum also occur. The FTIR spectra of the studied coal samples show weak organic functional group bands, which are obscured due to partial overlapping with intensive silicates bands. The organic coal components are mostly observed in the aliphatic and aromatic bands regions. The most abundant mineral in all shale samples is quartz, tab. S4 in the *Supplementary material*, accompanied by clay minerals and dolomite. Aragonite occasionally occurs in small amounts. Clay minerals include illite, dioctahedral smectite, and chlorite.

Geochemistry

Variations of the SiO_2, Fe_2O_3, Al_2O_3, CaO and SO_3 contents, tab. 3 and tab. S5, in the *Supplementary material*, in the coal samples are obvious in each deposit and depend on mineral matter content. Generally, high temperature coal ash from Jarando, Progorelica, and most samples from Tadenje deposit display high SiO_2 contents, followed by Al_2O_3, TiO_2, Fe_2O_3, and low Na_2O, K_2O, and P_2O_5 contents. Coal ash from the lower part of Seam 5 of the Tadenje deposit (Tadenje 10A, Tadenje 10B) has high CaO (32.33-45.63%), Fe_2O_3 (10.30-17.96%) and SO_3 (14.31-14.94%) contents, and low SiO_2 (17.99-22.64%) content. The highest Fe_2O_3 (49.78%) was observed in Tadenje Seam 3.

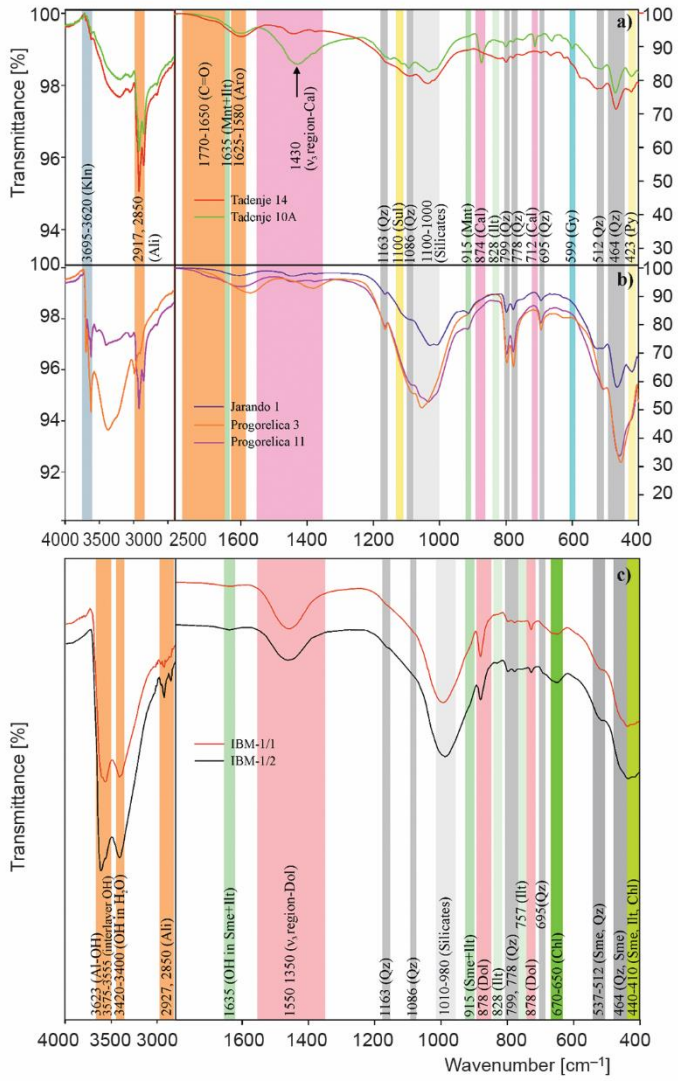

Figure 4. The FTIR spectra of the coal (a)-(b) samples from Tadenje, Progorelica, and Jarando, and shale (c) samples from Piskanja boron deposit; *OH-region and aliphatic organic component regions (2800-3800 cm-1) are shown at the left pane, fingerprint region of (1800-400 cm-1) is shown at the right pane.* Abbreviations [23]: *Qz – quartz, Kln – kaolinite, Mnt – montmorillonite, Ilt – illite, Chl – chlorite, Sme – smectite, Cal – calcite, Dol – dolomite, Sul – sulphates, Py – pyrite, Gy – gypsum, Arg? – aragonite, Ali – aliphatic components, Aro – aromatic components, C=O – oxygenated functional groups region*
(*for color image see journal web site*)

The HTCA from the Ibar Basin is highly enriched in As, Cr and Ni in comparison with the Clarke values for ash in bituminous coals [24]. The highest content of As (852.7 ppm; tab. S6, in the *Supplementary material*), Cr (294.3 ppm), Ni (1025.6 ppm), V (272.2 ppm), Cu (137.2 ppm), Mo (45.5 ppm), Sb (21.7 ppm), Sr (1520 ppm) and Pb (91.7 ppm) observed in HTCA from Tadenje deposit, while the highest contents of Cd (2.4 ppm), Co (145.1 ppm) and Mn (763 ppm) were determined in the Jarando HTCA.

Table 3. Contents of major oxides [%] and trace elements [ppm] of the high temperature coal ash and shale samples from the Ibar Basin

Elements	Min_{coal}	Max_{coal}	AV_{coal}	Min_{shale}	Max_{shale}	AV_{shale}	Clarke values of bituminous coal ash, ppm [23]	Clarke values of black shales, ppm [23]
SiO_2	18.0	78.8	**54.3**	50.2	62.3	**56.2**		
Al_2O_3	3.6	19.3	**11.5**	12.6	19.4	**14.8**		
Fe_2O_3	3.2	49.8	**14.5**	6.0	7.9	**6.7**		
TiO_2	0.2	0.5	**0.4**	0.5	0.9	**0.6**		
SO_3	0.8	14.9	**5.0**	0.1	0.4	**0.2**		
CaO	0.9	45.6	**9.1**	1.5	13.1	**6.9**		
MgO	0.3	2.0	**0.9**	3.9	14.2	**8.6**		
Na_2O	0.1	1.0	**0.5**	1.6	3.5	**2.4**		
K_2O	0.3	1.6	**1.0**	2.4	4.3	**3.2**		
P_2O_5	0.1	0.8	**0.3**	0.1	0.2	**0.1**		
As	31	853	**168**	19	225	**65**	46 ±5	30 ±3
Ba	168	699	**401**	391	723	**544**	980 ±60	500 ±20
Be	1	11	**5**	1	2	**2**	12 ±1	2.0 ±0.1
Cd	0.2	2.4	**0.7**	0.5	2.6	**0.9**	1.2 ±0.3	5.0 ±0.6
Co	2	145	**34**	19	32	**27**	37 ±2	19 ±1
Cu	33	137	**77**	64	338	**142**	110 ±5	70 ±3
Cr	41	294	**132**	142	275	**217**	120 ±5	96 ±3
Ni	14	1026	**295**	109	273	**214**	100 ±5	70 ±2
Mn	19	763	**179**	508	2662	**1425**	430 ±30	400 ±20
Mo	7	46	**22**	2	29	**9**	14 ±1	20 ±1.5
Sb	2	22	**8**	2	32	**10**	7.5 ±0.6	5.0 ±0.5
Sr	140	1520	**389**	195	1285	**776**	730 ±50	190 ±10
Pb	10	92	**33**	90	718	**239**	55 ±6	21 ±1
V	10	272	**163**				170 ±10	205 ±15
Zn	13	312	**94**	119	555	**210**	170 ±10	130 ±10

Min – minimum value, Max – maximum value, and AV – arithmetic mean value

The shale from the Piskanja deposit displays high SiO_2, tab. 3, lower Al_2O_3 and variable MgO and CaO contents. The highest content of MgO is determined in the upper most part of the Piskanja deposit (IBM-1/1), while the highest CaO is determined in the sample from 195.4-196.6 m depth (IBM-1/7). Shales are highly enriched in Cu, Cr, Ni, Mn, Sr, and Pb in comparison with Clarke values for black shales [24].

Discussion

Minerals in coal play a significant role in coal utilisation, from exploitation, grinding, washing, combustion, coking, to the environmental and human health impacts [1, 25]. Their presence has a negative economic impact and reduces the coal price if it is necessary to use coal cleaning processes before combustion or coke production. The mineralogical composition of coal influences the contents of fly ash, bottom ash and slag, and the gaseous products as well. Several optical methods and chemical analyses are applied for determining the mineralogical and geochemical compositions of coal [26, 27]. Statistical treatment of data obtained by these analyses, is also applied for assessing the modes of occurrence of major/minor and trace elements in sedimentary rocks and coal.

Mineralogical analyses revealed that the Jarando, Progorelica and Tadenje coals from the Ibar Basin are characterised by high content of silicates and aluminosilicates, pyrite, Fe-Mg-sulphate, and carbonate minerals. Silicate and aluminosilicate minerals include mainly quartz and clay minerals, while plagioclase and mica were rarely observed, tabs. 1 and S4. Quartz is a major mineral component occurring as single angular to semi-rounded grains of detrital origin [26, 27]. Dominant clay mineral in coal samples is kaolinite, accompanied by dioctahedral smectite, rarely illite and interstratified smectite-chlorite-vermiculite. Clay minerals are mostly of detrital origin [26], except kaolinite, which does not occur within the basin sedimentary sequence, indicating a rather diagenetic origin. Kaolinite may have formed due to weathering and/or hydrothermal alteration of feldspar, mica, smectite, and illite from the surrounding granitic basement. The detrital plagioclase and biotite, likely sourced from neighbouring granitoid masses, occur as an irregularly shaped crystals, usually in association with plagioclase in clay-rich layers. Pyrite is one of the most abundant sulphide minerals with variable content implying reducing depositional conditions. Syngenetic pyrite was observed in all coal samples as framboidal and euhedral crystals [28] along stratified bands or infilling cavities within the organic matter. Epigenetic pyrite was determined within cleats and fractures in the organic matrix. Several pyrite grains from Tadenje deposit (sample Tadenje 11) contain As and Ni as observed in SEM-EDS. This is in accordance with the geochemical composition of HTCA tab. S5 in the *Supplementary material*. Sphalerite was detected in the Jarando deposit in small amounts. Gypsum and szomolnokite/kieserite were determined only in Tadenje deposit, of authigenic, mainly epigenetic origin, formed as weathering products [29]. Szomolnokite most probably formed as secondary mineral from pyrite, implying highly acidic, oxic and arid conditions during the formation of that part of the coal seam. Barite was determined in very low amounts and is mostly enriched in Sr. The Fe oxides/hydroxides are present in considerable amounts in the Progorelica 3 Upper Seam and are probably the result of the weathering of Fe-rich minerals such as pyrite and siderite, whereas small amount of these minerals might be of detrital origin. Rutile/anatase was observed in low amount in Jarando coal as small aggregates with low V content. The most abundant carbonate mineral in the Ibar coal is calcite. Calcite is present in high amounts in the lower part of Seam 5 in Tadenje deposit as individual rounded and angular grains and spherical aggregates, implying probably their syngenetic origin. Small amount of ankerite occurs as small angular grains in Tadenje deposit. Borates are present in almost all examined coal fractions, associated with coal and clays. They are usually light yellow and, most likely, correspond to howlite, colemanite, jarandolite and ulexite [5].

The major oxide contents of the HTCA are compatible with identified silicate and aluminosilicate minerals rich in SiO_2, Al_2O_3, K_2O, and TiO_2. High to relatively high content of Fe_2O_3 in the HTCA can be related to pyrite and Fe-sulphate minerals present in coals. High

CaO content in HTCA in the lower part of Tadenje Seam 5 is in accordance with calcite as a major mineral phase observed through XRD, SEM-EDS, and FTIR analyses. Higher content of SO_3 and Fe_2O_3 in the same samples is compatible with the mineral association of calcite, gypsum, szomolnokite/kieserite.

The Piskanja borate deposit is characterised by a thick monotonous sequence of mudstones/marlstones, and it is likely stratigraphically younger than coal seams in Progorelica and Tadenje. The studied samples represent organic-rich lacustrine and alluvial sediments with silicates and aluminosilicates as the most abundant minerals with variable content of carbonate minerals. The clastic material resulted from the weathering, erosion, and transport from the surrounding basement rocks. Quartz and clay minerals (illite, smectite, chlorite) are major mineral phases in shales with variable content of plagioclase, and dolomite as major carbonate mineral. Mica (muscovite and biotite) and zeolite minerals are rare. Pyrite is the most abundant sulphide mineral but in low amount compared to coal. Lead, Zn, and Cu sulphide minerals are also included in the deepest part of the deposit and correspond to the highest contents of As, Cd, Sb, Pb, and Zn, tab. S5 in the *Supplementary material*. The highest content of Mn is also noticed in the same part. Mineralogical and geochemical compositions are in accordance and imply variation in the depositional environment and local climatic conditions as well as post-depositional hydrothermal phases in the Ibar Basin.

Although the studied coals and shales in the subbasins of Jarando Basin are dominantly deposited in marshes surrounding the basin under reducing and humid climatic conditions [4, 6], our data show internal variations from this trend. In particular, the documented variations in coal mineralogy and geochemistry imply that aforementioned conditions have been interrupted by short phases when the succession was exposed to oxic and dry conditions.

Conclusions

The Jarando, Progorelica and Tadenje coals are characterised by high content of quartz and clay minerals and lower amount of plagioclase and mica. The dominant clay mineral in coal is kaolinite, accompanied by smectite, rarely illite and interstratified smectite-chlorite-vermiculite. Pyrite is the most abundant sulphide mineral with variable content of Ni and As. Small amount of sphalerite is also included. Gypsum and szomolnokite/kieserite are the most common sulphate minerals in Tadenje deposit, whereas barite mostly enriched in Sr, is less abundant. The Fe oxides/hydroxides occur in considerable amounts in the Progorelica deposit while rutile/anatase is present in Jarando coal in low amount. Calcite is the most abundant carbonate mineral, especially in the lower part of Seam 5 in Tadenje deposit, where also ankerite occurs in small amount. The major oxide composition of the HTCA is compatible with the mineral association in coal.

The organic-rich shale from the Piskanja deposit is characterised by high content of silicates and aluminosilicates with variable content of carbonate minerals. The most abundant silicate minerals are quartz and clay minerals, with lower content of plagioclase and mica. Dolomite is the most abundant carbonate mineral, especially in the upper part of deposit. The mineral association is in accordance with the major oxide composition and the trace element contents.

Acknowledgment

This work was financially supported by the Ministry of Science, Technological Development and Innovation of the Republic of Serbia (Contract number: 451-03-66/2024-03/200052, 451-03-66/2024-03/200053, and 451-03-65/2024-03/200126) as well as by the

Deutsche Forschungsgemeinschaft (DFG) DRASTIC grant to Nevena Andrić-Tomšević (grant number TO 1364/3-1).

Authors are also grateful to the reviewers Prof dr Kimon Christanis and Prof dr Ksenija Stojanović, Editor-in-Chief, Dr. Vukman Bakić and Prof dr Simeon Oka and Guest Editor, Prof. Dr. Marko Obradović, whose constructive comments and suggestions greatly improved this manuscript.

Supplementary Material

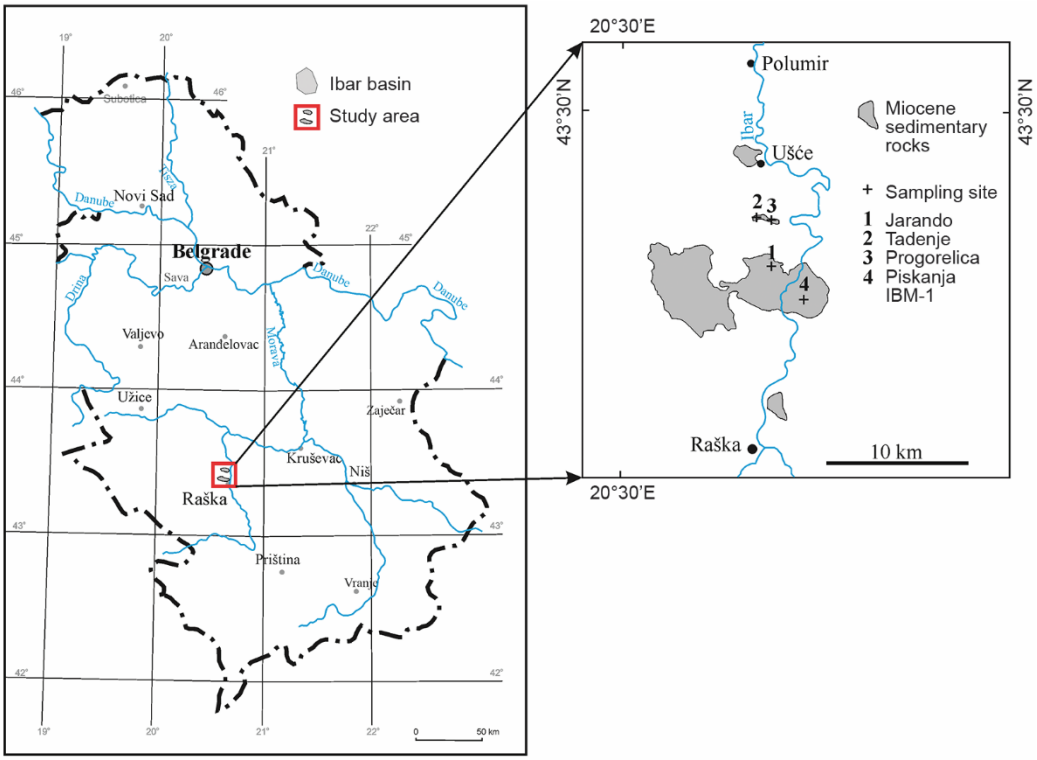

Figure S1. Location of the Ibar Basin and the sampling sites

Table S1. The samples collected from the Ibar Basin

Mine/ deposit	Latitude-longitude [°]	Sample ID	Lithology	Seam	Depth [m]	Analytical technique applied
Jarando	N 43.40264 E 20.62593	Jarando 1	Coal	6	296.0-296.5	ICP-MS, XRD, SEM-EDS, FTIR
		Jarando 3	Coal	6	297.3-297.9	ICP-MS, XRD, SEM-EDS, FTIR
Tadenje	N 43.43155 E 20.61397	Tadenje 11	Coal	3	47.6-48.6	ICP-MS, XRD, SEM-EDS, FTIR
		Tadenje 14	Coal	3	49.6-50.3	ICP-MS, XRD, SEM-EDS, FTIR
		Tadenje 1	Coal	5	68.4-68.6	ICP-MS, XRD, SEM-EDS, FTIR
		Tadenje 10A	Coal	5	70.5-70.7	ICP-MS, XRD, SEM-EDS, FTIR
		Tadenje 10B	Coal	5	70.7-71.0	ICP-MS, XRD, SEM-EDS, FTIR
Progorelica	N 43.43093 E 20.62405	Progorelica 3	Coal	Upper	2.2-2.7	ICP-MS, XRD, SEM-EDS, FTIR
		Progorelica 5	Coal	Upper	4.3-5.8	ICP-MS, XRD, SEM-EDS, FTIR
		Progorelica 1	Coal	Main	17.8-18.0	ICP-MS, XRD, SEM-EDS, FTIR
		Progorelica 10	Coal	Main	20.3-21.3	ICP-MS, XRD, SEM-EDS, FTIR
		Progorelica 16	Coal	Main	33.8-34.3	ICP-MS, XRD, SEM-EDS, FTIR
		Progorelica 11	Coal	Main	42.3-43.1	ICP-MS, XRD, SEM-EDS, FTIR
Piskanja	N 43.38174 E 20.65376	IBM-1/1	Shale		43.5-44.5	XRF, ICP-MS, SEM-EDS, FTIR
		IBM-1/2	Shale		47.0-47.9	XRF, ICP-MS, XRD, SEM-EDS, FTIR
		IBM-1/3	Shale		63.2-66.8	XRF, ICP-MS, XRD, SEM-EDS, FTIR
		IBM-1/4	Shale		122.8-123.9	XRF, ICP-MS, XRD, SEM-EDS, FTIR
		IBM-1/6	Shale		127.0-128.2	XRF, ICP-MS, SEM-EDS, FTIR
		IBM-1/7	Shale		195.4-196.6	XRF, ICP-MS, XRD, FTIR
		IBM-1/8	Shale		226.3-227.6	XRF, ICP-MS, XRD, SEM-EDS, FTIR
		IBM-1/27	Shale		344.2-344.5	XRF, ICP-MS, XRD, SEM-EDS, FTIR
		IBM-1/29	Shale		352.2-353.2	XRF, ICP-MS, SEM-EDS, FTIR

Table S2. The FTIR absorption bands of coal samples spectra from Tadenje, Jarando, and Progorelica deposits in comparison with previously reported data

Frequency (measured) [cm^{-1}]	Second derivative [cm^{-1}]	Frequency (literature) [cm^{-1}]	Assignment	Compound	References
3695		3695	In-phase stretching mode of inner-surface OH groups	Kaolinite	30-32
3648		3651	Out-of-phase stretching modes of inner-surface OH groups		33, 31
3621-3620		3619	Stretching of the inner OH group		33, 31
	2965-2955	2954	$–CH_3$ asymmetric stretching	Aliphatic components	34
2919-2926	2923	2921, 2915-2923, 2918	$–CH_2$ asymmetric stretching		35
	2868-2867	2870	$–CH_3$ symmetric stretching		34
2850	2851	2851	$–CH_2$ symmetric stretching		35
	2820	2820	Unknown		34
1795		1795	v1+v4 vibrational modes	Calcite	36
		1705	Carboxyl acids	Oxygenated (C=O) functional groups	34
	1659-1657	1659	C=O		37
	1650-1649		Conjugated C=O		34, 38
1620-1596		1635	OH bending vibrations	Smectite, Illite	33
	1620		Aromatic C=C ring stretching	Aromatic components (*e.g*. lignin)	34, 38
	1613-1611				38
1600-1598	1599-1591	1606			35
1430		1427	v3(CO_3) asymmetric stretching	Calcite	36, 39
1375		1375	Tertiary butyl groups		40
1164-1162		1173-1170, 1175	v3(Si–O) asymmetrical stretching (Al/Si substitution)	Quartz	36, 41
1149-1090		1150-1080	v3(SO_4) asymmetrical stretching	Sulfates	36, 42, 43
1093-1086		1084, 1085-1081	v3(Si–O) asymmetrical stretching (Al/Si substitution)	Quartz	36, 41
1035-1026		1032	In-plane Si–O-Si stretching	Silicates	35
1008-1006		1009			35

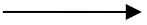

Table S2. continuation

Frequency (measured) [cm^{-1}]	Second derivative [cm^{-1}]	Frequency (literature) [cm^{-1}]	Assignment	Compound	References
915-913		915	Al–OH–Al bending	Montmori-llonite	33, 32
874		876	v2(CO_3) out-of-plane bending	Calcite	36
828		828	Al–OH–Mg bending	Illite	33
802-797		798, 801-797	v1(Si–O) symmetrical stretching	Quartz	36, 41
779-777		779-778, 782-778			36, 41
712		712	v4(CO_3) in-plane bending	Calcite	36, 39
695-694		696, 695-691	v2(Si–O) symmetrical bending	Quartz	36, 41
599	602	604	SO_4^{2-} bending	Gypsum	35
532		536, 538	Al–O–Si bending	Kaolinite	36, 35
512-507		513-512, 524-512	v2(Si–O) symmetrical bending	Quartz	36, 41
467-463		459, 462-457, 466-463	v4(Si–O) asymmetrical bending	Quartz	36, 41, 44
423-419		425, 425-422		Pyrite	42, 43

Table S3. The FTIR absorption bands of shale samples spectra from Piskanja boron deposit in comparison with previously reported data

Frequency (measured) [cm^{-1}]	Frequency (literature) [cm^{-1}]	Assignment	Mineral/compound	References
3674	3679-3671	Mg_3OH stretching	Chlorite	45
3620-3626	3619, 3622–3621	Stretching of the inner OH group	Smectite, Illite	
3575-3555		Interlayer oxy-hydroxyl sheets	Chlorite	45
3420-3400	broad band near 3420	OH stretching vibrations (in H_2O)	Smectite	45
2920	2921, 2915-2923, 2918	$–CH_2$ asymmetric stretching	Aliphatic component	35, 34
2853	2851	$–CH_2$ symmetric stretching		
1635	1635	OH bending vibrations	Smectite, Illite	33
1473-1437	1441	v3(CO_3) asymmetric stretching	Dolomite	46
1163	1173-1170, 1175	v3(Si–O) asymmetrical stretching (Al/Si substitution)	Quartz	36, 41
1083	1084, 1085-1081	v3(Si–O) asymmetrical stretching (Al/Si substitution)	Quartz	36, 41

Table S3. continuation

Frequency (measured) [cm^{-1}]	Frequency (literature) [cm^{-1}]	Assignment	Mineral/compound	References
1010-980	1032, 1009	In-plane Si–O-Si stretching	Silicates	36, 42
915	915	Al–OH–Al bending	Smectite, Illite	33, 32
878	881	v2(CO_3) out-of-plane bending	Dolomite	47
854	858-854	v2(CO_3) out-of-plane bending	Aragonite?	48
828	828	Al–OH–Mg bending	Illite	33
799	798, 801-797	v1(Si–O) symmetrical stretching	Quartz	36, 41
778	779-778, 782-778			36, 41
757	756	Al–O–Si in-plane	Illite	45
728	730	v4(CO_3) in-plane bending	Dolomite	47
695	696, 695-691	v2(Si–O) symmetrical bending	Quartz	36, 41
670-650	675-650	OH bending	Chlorite	45
537-512	534-520	Al–O–Si bending	Smectite	45
	513-512, 524-512	v2(Si–O) symmetrical bending	Quartz	36, 41
464	459, 462-457, 466-463	v4(Si–O) asymmetrical bending	Quartz	36, 41, 44
440-410		Si-O-Si bending	Smectite, Illite, Chlorite	45
423-419	425, 425-422		Pyrite	42, 43

Table S4. Mineralogical composition of coal and shale samples from the Ibar Basin, based on data from FTIR analysis

Sample ID	Minerals	Sample ID	Minerals
Jarando 1	Qz, Kln, Sme, Ilt, Py	Progorelica 16	Qz, Kln, Sme, Ilt, Py
Jarando 3	Qz, Kln, Sme, Ilt, Py	Progorelica 11	Qz, Kln, Sme, Ilt, Py
Tadenje 11	Qz, Kln, Sme, Ilt, Py	IBM-1/1	Qz, Dol, Sme, Ilt, Chl, Arg, Py
Tadenje 14	Qz, Kln, Sme, Ilt, Py	IBM-1/2	Qz, Dol, Sme, Ilt, Chl
Tadenje 1	Qz, Kln, Sme, Ilt, Cal, Py	IBM-1/3	Qz, Dol, Sme, Ilt, Chl, Arg, Py
Tadenje 10A	Qz, Kln, Sme, Ilt, Cal, Py, Gp	IBM-1/4	Qz, Sme, Ilt, Chl
Tadenje 10B	Qz, Kln, Sme, Ilt, Cal, Py, Gp	IBM-1/6	Qz, Dol, Sme, Ilt, Chl, Arg, Py
Progorelica 3	Qz, Kln, Sme, Ilt, Py	IBM-1/7	Qz, Sme, Ilt, Chl, Arg, Py
Progorelica 5	Qz, Kln, Sme, Ilt, Py	IBM-1/8	Qz, Sme, Ilt, Chl
Progorelica 1	Qz, Sme, Ilt, Py	IBM-1/27	Qz, Dol, Sme, Ilt, Chl
Progorelica 10	Qz, Kln, Sme, Ilt, Py	IBM-1/29	Qz, Dol, Sme, Ilt, Chl

Qz – quartz, Kln – kaolinite, Ilt – illite, Sme – smectite, Chl – chlorite, Arg – aragonite, Py – pyrite, Cal – calcite; Dol – dolomite, Gp – gypsum

Table S5. Content of major oxides [%] of individual samples in HTCA and shale samples from the Ibar Basin

Sample ID	SiO_2	Al_2O_3	Fe_2O_3	TiO_2	SO_3	CaO	MgO	Na_2O	K_2O	P_2O_5
Jarando 1	60.57	17.04	12.20	0.41	1.15	1.01	1.53	0.88	1.56	0.11
Jarando 3	61.89	14.15	12.83	0.46	1.17	1.01	1.18	0.78	1.53	0.13
Tadenje 11	40.58	11.47	31.50	0.47	6.40	5.83	0.84	0.67	0.88	0.43
Tadenje 14	31.58	10.00	49.78	0.30	2.41	3.17	0.66	0.41	1.18	0.09
Tadenje 1	43.14	15.65	16.45	0.42	5.46	8.58	1.99	1.04	1.38	0.78
Tadenje 10A	17.99	6.05	10.30	0.19	14.31	45.63	0.95	0.38	0.77	0.25
Tadenje 10B	22.64	8.75	17.96	0.29	14.94	32.33	0.78	0.71	0.87	0.40
Progorelica 3	73.34	5.40	3.18	0.20	7.96	8.74	0.48	0.12	0.26	0.19
Progorelica 5	67.77	13.90	3.81	0.41	4.47	5.48	0.81	0.11	0.79	0.21
Progorelica 1	78.79	3.64	10.99	0.29	1.60	1.99	0.33	0.32	0.49	0.66
Progorelica 10	63.70	19.29	8.22	0.50	0.97	0.90	0.83	0.13	1.15	0.26
Progorelica 16	70.06	14.71	7.89	0.33	0.77	0.85	0.69	0.15	0.73	0.21
Progorelica 11	73.66	9.68	3.23	0.41	2.85	2.33	0.62	0.14	1.20	0.20
IBM-1/1	50.21	12.60	6.04	0.54	0.32	10.86	14.19	1.83	2.72	0.17
IBM-1/2	51.93	13.13	6.04	0.78	0.44	8.99	13.43	1.72	3.23	<0.1
IBM-1/3	59.06	13.47	7.08	0.60	0.09	7.12	7.15	2.22	2.84	0.15
IBM-1/4	59.18	14.05	6.03	0.55	0.09	1.50	11.69	3.49	3.14	0.11
IBM-1/6	52.73	14.43	6.63	0.66	0.17	7.73	10.93	2.76	3.45	0.14
IBM-1/7	52.64	15.76	6.90	0.59	0.37	13.06	5.05	3.05	2.38	<0.1
IBM-1/8	59.40	15.60	7.89	0.48	0.09	3.77	6.38	2.67	3.49	<0.1
IBM-1/27	62.25	14.81	6.44	0.73	0.09	5.56	5.04	1.86	2.96	<0.1
IBM-1/29	58.45	19.39	7.42	0.86	0.09	3.42	3.95	1.63	4.34	<0.1
Min_{coal}	17.99	3.64	3.18	0.19	0.77	0.85	0.33	0.11	0.26	0.09
Max_{coal}	78.79	19.29	49.78	0.50	14.94	45.63	1.99	1.04	1.56	0.78
AV_{coal}	**54.29**	**11.52**	**14.49**	**0.36**	**4.96**	**9.07**	**0.90**	**0.45**	**0.98**	**0.30**
Min_{shale}	50.21	12.60	6.03	0.48	0.09	1.50	3.95	1.63	2.38	0.11
Max_{shale}	62.25	19.39	7.89	0.86	0.44	13.06	14.19	3.49	4.34	0.17
AV_{shale}	**56.20**	**14.81**	**6.72**	**0.64**	**0.19**	**6.89**	**8.65**	**2.36**	**3.17**	**0.14**

Table S6. Content of selected trace elements [ppm] of individual samples in HTCA and shale samples from the Ibar Basin

Sample ID	As	Ba	Be	Cd	Co	Cu	Cr	Ni	Mn	Mo	Sb	Sr	Pb	V	Zn
Jarando 1	75.2	485	4.3	0.4	20.8	57.6	57.0	78.1	232	6.7	1.9	350	30.4	130.8	88.0
Jarando 3	88.6	443	8.1	2.4	145.1	33.4	66.2	145.3	763	7.8	2.8	285	27.8	201.1	312.4
Tadenje 11	852.7	617	10.1	0.5	21.3	81.2	244.0	575.8	65	29.6	15.5	244	54.3	259.1	93.5
Tadenje 14	296.4	180	8.5	0.8	55.4	82.7	294.3	1025.6	89	30.4	20.0	140	73.9	272.2	76.6
Tadenje 1	130.7	276	11.1	1.0	49.5	137.2	278.6	731.9	256	45.5	21.7	287	91.7	208.1	187.3
Tadenje 10A	56.0	168	2.7	0.6	28.5	62.8	124.3	327.1	315	29.2	14.2	1520	32.8	237.8	78.6
Tadenje 10B	<2.3	262	5.7	0.6	50.4	85.5	176.3	637.4	293	<1.0	<1.5	793	19.9	10.5	105.4
Progorelica 3	31.4	699	1.0	<0.10	2.7	60.5	40.6	19.6	25	8.4	1.7	279	10.0	41.4	24.5
Progorelica 5	57.9	475	1.0	<0.10	1.8	122.9	68.2	14.1	19	16.3	2.4	254	21.0	99.6	13.3
Progorelica 1	122.6	582	6.5	0.2	6.2	126.8	133.4	47.2	51	25.7	1.7	186	11.0	233.8	21.9
Progorelica 10	127.5	367	1.2	0.2	24.4	75.5	58.3	91.3	82	17.0	3.5	271	17.3	168.3	91.0
Progorelica 16	122.2	394	1.8	0.2	26.6	39.8	61.7	107.7	70	22.5	2.6	203	16.4	110.3	108.3
Progorelica 11	49.1	269	1.6	<0.10	5.1	32.5	110.2	34.5	63	23.7	4.9	245	20.2	151.8	23.0
IBM-1/1	31.6	613	1.7	0.7	29.0	337.5	203.7	253.8	1581	21.2	4.6	1103	105.3		123.2
IBM-1/2	19.1	529	1.6	0.6	25.3	158.0	191.3	185.7	1405	29.0	2.2	1212	95.4		118.8
IBM-1/3	20.3	473	2.4	0.5	28.1	129.4	243.3	240.2	1712	3.9	5.9	667	134.4		154.3
IBM-1/4	26.3	600	1.4	0.6	31.5	138.6	274.6	273.0	508	4.7	4.0	1073	122.2		149.9
IBM-1/6	28.2	723	1.8	0.6	27.3	108.7	196.4	189.5	1660	14.0	3.7	1285	90.0		124.8
IBM-1/7	24.8	440	1.7	0.5	27.8	124.7	242.1	250.4	705	4.5	4.5	775	122.7		130.6
IBM-1/8	33.3	582	2.1	0.9	30.3	138.0	270.7	264.4	1207	2.9	9.3	240	364.9		229.6
IBM-1/27	173.5	391	1.7	1.3	18.6	81.9	142.2	109.1	1386	1.9	25.7	435	395.5		304.6
IBM-1/29	225.3	551	2.2	2.6	23.1	64.2	185.6	163.9	2662	1.8	32.0	195	718.3		555.4
Min_{coal}	31.4	168	1.0	0.2	1.8	32.5	40.6	14.1	19	6.7	1.7	140	10.0	10.5	13.3
Max_{coal}	852.7	699	11.1	2.4	145.1	137.2	294.3	1025.6	763	45.5	21.7	1520	91.7	272.2	312.4
AV_{coal}	**167.5**	**401**	**4.9**	**0.7**	**33.7**	**76.8**	**131.8**	**295.0**	**179**	**21.9**	**7.7**	**389**	**32.8**	**163.4**	**94.1**
Min_{shale}	19.1	391	1.4	0.5	18.6	64.2	142.2	109.1	508	1.8	2.2	195	90.0		118.8
Max_{shale}	225.3	723	2.4	2.6	31.5	337.5	274.6	273.0	2662	29.0	32.0	1285	718.3		555.4
AV_{shale}	**64.7**	**544**	**1.8**	**0.9**	**26.8**	**142.3**	**216.7**	**214.4**	**1425**	**9.3**	**10.2**	**776**	**238.7**		**210.1**

References

[1] Dai, S., *et al., Inorganic Geochemistry of Coal*, Elsevier, Amsterdam, The Netherlands, 2023
[2] Miller, B. G. *Clean coal engineering technology*, 2nd edn. Elsevier, Amsterdam, The Netherlands, 2016
[3] Hower, J. C., *et al*., Understanding Coal Quality and the Critical Importance of Comprehensive Coal Analyses, *International Journal of Coal Geology*, *263* (2022), 104120

[4] Ercegovac, M., *et al*., Petrological and Geochemical Studies of the Coals of the Ibar River Basin (Yugoslavia) (in German), *International Journal of Coal Geology, 111* (1991), 19, pp. 5-22
[5] Obradović, J., Vasić, N., *Neogene Lacustrine Basins from Serbia*, Serbian Academy of Science and Arts, Belgrade, Serbia 2007
[6] Andrić, N., *et al*., The Thermal History of the Miocene Ibar Basin (Southern Serbia): New Constraints from Apatite and Zircon Fission Track and Vitrinite Reflectance Data, *Geologica Carpatica, 66* (2015), 1, pp. 37-50
[7] Đorđević, Ž., Das Tertiäre Ibar-Becken (in Serbian), *Proceedings of the Serbian Geological Society*, Belgrade, Serbia, pp. 97-100, 1954
[8] Pantić, N., Age of the Coal-Bearing Sedimentary Series near JARANDOL (valley of the river Ibar) on the Basis of the Latest Paleofloral Data (in Serbian), *Bulletin of Institute for geological and geophysical exploration*, XIX (1961), A, pp. 287-297
[9] Ćirić, A., Über den Fund der *Art Mastodon (Bunolophodon) Angustidens Cuv. F. Subtapirodea Schles.* in der Braunkohlengrube Jarando bei Raška (in Serbian and German), *Bulletin of Institute for geological and geophysical exploration*, XX (1962), A, pp. 103-106
[10] ***, Basic Geologic Map of Serbia, section K34-18, https://geoliss.mre.gov.rs/prez/OGK/ RasterSrbija
[11] ***, Basic Geologic Map of Serbia, section K34-30, https://geoliss.mre.gov.rs/prez/OGK/ RasterSrbija
[12] Harzhauser, M., Mandić, O., Neogene Lake Systems of Central and South-Eastern Europe: Faunal Diversity, Gradients and Interrelations, *Palaeogeography, Palaeoclimatology, Palaeoecology, 260* (2008), 3-4, pp. 417-434
[13] Andrić-Tomašević, *et al*., An Arid Phase in the Internal Dinarides During the Early to Middle Miocene: Inferences from Mg-Clays in the Pranjani Basin (Serbia), *Palaeogeography, Palaeoclimatology, Palaeoecology, 562* (2021), 110145
[14] Schmid, S. M., *et al*., The Alpine-Carpathian-Dinaridic Orogenic System: Correlation and Evolution of Tectonic Units, *Swiss Journal of Geosciences, 101* (2008), Mar., pp. 139-183
[15] Stojadinović, U., *et al*., The Balance between Orogenic Building and Subsequent Extension during the Tertiary Evolution of the NE Dinarides: Constraints from Low-Temperature Thermochronology, *Global and Planetary Change 1, 103* (2013), Apr., pp. 19-38
[16] Andrić, N., *et al.*, The Link between Tectonics and Sedimentation in Asymmetric Extensional Basins – Inferences from the Study of the Sarajevo-Zenica Basin, *Marine and Petroleum Geology, 83* (2017), May, pp. 305-332
[17] Schefer, S., Tectono-Metamorphic and Magmatic Evolution of the Internal Dinarides (Kopaonik Area, Southern Serbia) and Its Significance for the Geodynamic Evolution of the Balkan Peninsula, Ph. D. thesis, University of Basel, Basel, Switzerland, 2010
[18] Matović, V., *et al*., *Sedimentary Rock Testing Methods*, University of Begrade, Faculty of Mining and Geology, Begrade, Serbia, 2019
[19] Menges, F., *Spectragryph – Optical Spectroscopy Software*, Version 1.2.16.1, 2022, http://www.effemm2.de/spectragryph/
[20] ***, ISO 7404-2, 2009. Methods for the Petrographic Analysis of Coals — Part 2: Methods of Preparing Coal Samples. International Organization for Standardization, Geneva, Switzerland, (2009)
[21] ***, ASTM D6357-21a, Determination of Trace Elements in Coal, Coke and Combustion Residues from Coal Utilization Processes Using ICP-AES, ICP-MS and GFAAS, American Society for Testing and Materials, Philadelphia, USA, 2021
[22] ***, ASTM D6349-21, Determination of Major and Minor Elements in Coal, Coke and Solid Residues from Combustion of Coal and Coke by Using ICP-AES, American Society for Testing and Materials, Philadelphia, USA, 2021
[23] Whitney, D. L.**,** Evans, B. W., Abbreviations for Names of Rock-Forming Minerals, *American Mineralogist, 95* (2010), 1, pp. 185-187
[24] Ketris, M. P., Yudovich, Y. A. E., Estimations of Clarkes for Carbonaceous Biolithes: World Averages for Trace Element Contents in Black Shales and Coals, *International Journal of Coal Geology, 78* (2009), 2, pp. 135-148
[25] Dai, S., *et al*., Geochemistry of Trace Elements in Chinese Coals: a Review of Abundances, Genetic Types, Impacts on Human Health, and Industrial Utilization, *International Journal of Coal Geology, 94* (2012), May, pp. 3-21
[26] Finkelman, R. B., *et al*., The Importance of Minerals in Coal as the Hosts of Chemical Elements: A Review, *International Journal of Coal Geology, 212* (2019), 103251

[27] Ward, C. R., Analysis, Origin and Significance of Mineral Matter in Coal: an Updated Review, *International Journal of Coal Geology, 165* (2016), Aug., pp. 1-27
[28] Chou, C.-L., Sulfur in Coals: A Review of Geochemistry and Origins, *International Journal of Coal Geology, 100* (2012), Oct., pp. 1-13
[29] Dai, S., *et al*., Recognition of Peat Depositional Environments in Coal: A Review, *International Journal of Coal Geology, 219* (2020), 103383
[30] Srodon, J., Identification and Quantitative Analysis of Clay Minerals, in: (F. Bergaya and G. Lagaly Editors), 5, Handbook of Clay Science, Elsevier, Amsterdam, The Netherlands, 2013, pp. 25-49
[31] Balan, E., *et al*., First-Principles Study of OH-Stretching Modes in Kaolinite, Dickite, and Nacrite, *American Mineralogist*, *90*, (2005), 1, pp. 50-60
[32] Srasra, E., *et al*., Infrared Spectroscopy Study of Tetrahedral and Octahedral Substitutions in an Interstratified Illite-Smectite Clay, *Clays and Clay Minerals, 42* (1994), 3, pp. 237-241
[33] Muller, C., *et al*., Infrared Attenuated Total Reflectance Spectroscopy: An Innovative Strategy for Analyzing Mineral Components in Energy Relevant Systems, *Scientific Reports, 4* (2014), 1, 6764
[34] Ibarra, J. V., *et al*., FTIR Study of the Evolution of Coal Structure during the Coalification Process, *Organic Geochemistry, 24* (1996), 6, pp. 725-735
[35] Yin, Y., *et al*., Characterization of Coals and Coal Ashes with High Si Content Using Combined Second-Derivative Infrared Spectroscopy and Raman Spectroscopy, *Crystals, 10* (2019), 9, 513
[36] Chukanov, N. V., *Infrared Spectra of Mineral Species, Springer Mineralogy*, Springer International Publishing, Cham, New York, USA, 2014
[37] Li, K., *et al*., Comprehensive Investigation of Various Structural Features of Bituminous Coals Using Advanced Analytical Techniques, *Energy & Fuels, 29* (2015), 11, pp. 7178-7189
[38] Craddock, P., *et al*., Evolution of Kerogen and Bitumen during Thermal Maturation *via* Semi-Open Pyrolysis Investigated by Infrared Spectroscopy, *Energy & Fuels, 29* (2015), 4, pp. 2197-2210
[39] Luzinova, Y., *et al*., Detection of Cold Seep Derived Authigenic Carbonates with Infrared Spectroscopy, *Marine Chemistry, 125* (2011), 1-4, pp. 8-18
[40] Balachandran, M., Role of Infrared Spectroscopy in Coal Analysis – An Investigation, *American Journal of Analytical Chemistry, 5* (2014), 6, pp. 367-372
[41] Saikia, B. J., *et al*., Fourier Transform Infrared Spectroscopic Estimation of Crystallinity in SiO_2 Based Rocks, *Bulletin of Material Science, 31*, (2008), Nov., pp. 775-779
[42] Chukanov, N. V., Chervonnyi, A. D., *Infrared Spectroscopy of Minerals and Related Compounds*, Springer Mineralogy, Springer International Publishing, Cham, New York, USA, 2016
[43] Dunn, J. G., *et al*., A Fourier Transform Infrared Study of the Oxidation of Pyrite, *Thermochimica Acta*, *208* (1992), Oct., pp. 293-303
[44] Saikia B. J., Spectroscopic Estimation of Geometrical Structure Elucidation in Natural SiO_2 Crystal, *Journal of Materials Physics and Chemistry*, *2* (2014), 2, pp. 28-33
[45] Madejova, J., *et al*., Chapter 5 – IR Spectra of Clay Minerals, in: (W. P. Gates, J. T. Kloprogge, J. Madejova and F. Bergaya eds.), *8, Developments in Clay Science*, Elsevier, Amsterdam, The Netherlands, 2017, pp. 107-149
[46] Chester, R., Elderfield, H., The Application of Infra-Red Absorption Spectroscopy to Carbonate Mineralogy, *Sedimentology, 9* (1967), 1, pp. 5-21
[47] Reig, F., *et al*., FTIR Quantitative Analysis of Calcium Carbonate (Calcite) and Silica (Quartz) Mixtures Using the Constant Ratio Method, *Application to Geological Samples, Talanta, 58* (2002), 4, pp. 811-821
[48] Chakrabarty, D., Mahapatra, S., Aragonite Crystals with Unconventional Morphologies, *Journal of Materials Chemistry, 11* (1999), 9, pp. 2953-2957

Paper submitted: April 5, 2024
Paper revised: May 7, 2024
Paper accepted: May 27, 2024